Cerium doped cobalt chromate for resistive and capacitive humidity sensor applications

V. Jagadeesha Angadi[1,*] , Kamaludin Abdulvakhidov[2], Nikolay Lyanguzov[3], Anuj Kumar[4], Himanshu Payal[5,6], Chander Prakash[7], Bidhan Pandit[8], and Mohd Ubaidullah[9,*]

[1] *Department of Physics, P.C. Jabin Science College, Hubballi 580031, India*

[2] *Southern Federal University, Sladkova, 178/24, Rostov-on-Don, Russia 344090*

[3] *Faculty of Physics, Southern Federal University, Zorge, 5, Rostov-on-Don, Russia 344090*

[4] *Department of Chemistry, GLA University, Mathura 281406, India*

[5] *Department of Mechanical Engineering, Sharda School of Engineering and Technology, Sharda University, Greater Noida, India*

[6] *Chitkara Centre for Research and Development, Chitkara University, Himachal Pradesh 174103, India*

[7] *Centre for Research Impact and Outcomes, Chitkara University, Rajpura, Punjab 140401, India*

[8] *Department of Materials Science and Engineering and Chemical Engineering, Universidad Carlos III de Madrid, Avenida de la Universidad 30, 28911 Leganés, Madrid, Spain*

[9] *Department of Chemistry, College of Science, King Saud University, P.O. Box 2455, 11451 Riyadh, Saudi Arabia*

ABSTRACT

The effect of cerium (Ce^{3+}) on the structural, microstructural, Fourier infrared spectroscopic, electrical, and humidity sensing behavior of $CoCr_{2-x}Ce_xO_4$(CoCrCe) is reported in this paper. To prepare the samples, Solution combustion method using mixture of urea and glucose as a fuel. Samples are sintered for 600 °C for 3 h to get single phase. To analyses the creatinine nature and morphology, samples were characterize X-ray diffraction (XRD) and scanning electron microscopy. XRD reveals that formation of cubic spinel structures with typical crystallite sizes of less than 10 nm. When Ce^{3+} ions are replaced by Cr^{3+} ions, the lattice parameter found decreases from 8.3289 to 8.3163 Å. This is due to the creation of a compressive lattice strain and may be due to the differences between ionic radius of Ce^{3+} as compared to Cr^{3+}. We discovered the chrommate structure in the absence of impurities by analysing the octahedral and tetrahedral stretching bands using Fourier infrared spectroscopy. Scanning Electron microscopy results reveals that samples exhibits highly porous nature. Elemental analysis were confirms the Ce^{3+} is present in the samples. All samples subjected to study the humidity sensing studies. The relative humidity influences the resistivity of the surrounding air significantly. We also investigated the relative permittivity characteristics, the conductivity of the samples of interest, and the capacitive sensor's response time at a fixed frequency of $f = 1$ kHz. Further, The variation of both relative permittivity and electrical resistivity were strongly depending on humidity. As concentration of Ce^{3+} increases the permittivity (unit less), Conductivity, electrical capacity(normalized), Response time of capacitive sensor were found increases such as 150, 10^8 [Ω m], 10, 90

Address correspondence to E-mail: jagdeeshbub@gmail.com; mtayyab@ksu.edu.sa

Springer

this is may be due to the larger ionic radius of the Ce^{3+} and also may be high porosity of the samples. Ce^{3+} at 2 mol% has improved humidity sensing properties as compared to other concentration. We conclude that $CoCr_{1.98}Ce_{0.02}O_4$ be useful for an active material in humidity-sensing devices.

1 Introduction

Spinel Chromates have received the majority of the focus in recent years when it comes to multiferroics materials. This is due to spinel chromates exhibits' extraordinary combination of structural, magnetic, multiferroics and dielectric properties [1–4]. $CoCr_2O_4$ has been used as a dye, a catalyst, and a base for growing films [5]. But only a few papers have talked about how $CoCr_2O_4$ and rare earth doped $CoCr_2O_4$ are made and what humidity properties they have [5–9]. Several experiments have shown that the nano size effect, surface-pinning issues, lattice distortion, and surface flaws are the main things that affect the magnetic properties of $CoCr_2O_4$ [4–9].But there is no reports avilbel in the literature Ce^{3+} doped $CoCr_2O_4$ for humidity properties. As people become more concerned about the environment, they are placing a greater emphasis on sensors [9–14]. Accurate humidity monitoring is required for a variety of reasons, including but not limited to agriculture, manufacturing, food storage, interior and outdoor air quality, and the quality of other interconnected industries. In addition to their technological significance, chromate materials have demonstrated advantages in the sensor industry due to their mechanical strength, chemical resistance, and stability. The spinel structure of chromates is primarily utilised in gas [1–3], stress and humidity [4] sensors. In industries such as textile dryers, air coolers, grill forming, cereal stockings and medicine, humidity sensors may be in demand [6]. Metal oxide-based humidity sensors have advantages such as low cost, straightforward construction, and ease of installation in the operating environment. The interaction between water molecules and the surface of a rare earth, i.e. the surface's reactivity, determines a rare earth's ability to detect the presence of water molecules [15–25]. A good humidity sensor should possess a variety of qualities, including sensitivity, chemical and thermal stability, reversibility, and reaction speed. Due to their many advantageous properties, spinel rare earth doped chromates are ideal candidates for use in applications involving humidity sensing. Cerium is diamagnetic material it will helps to improve the porosity of the samples. These benefits include their porous structure, high surface-to-volume ratio, humidity-variable resistivity, low cost,

straightforward synthesis, and adaptability to a wide range of operating conditions. Synthesis of porous materials is also uncomplicated. Because of their porous structure and high surface-to-volume ratio, chromates are an excellent choice for use as humidity sensors. Chemically speaking, the formula for spinel cubic chromate is $(AB_2)O_4$. The letter "B" refers to the octahedral shape, whereas the letter "A" refers to the tetrahedral shape. In the spine, cations A^{2+} are found in tetrahedral locations, whereas cations B^{3+} are found in octahedral locations. Due to their chemical stability, chromites are indispensable to the sensor and electronic industries [26]. The typical stoichiometric structure of spinel is subjected to a number of substantial modifications or substitutions with metal ions in order to achieve maximum performance. Due to the higher thermal and chemical stability of CoCrCe materials, we planned to use rare earth (Ce^{3+}) doped $CoCr_2O_4$ in the humidity study we were conducting.

The structure, microstructure, Fourier infrared, electrical, and humidity sensing behaviour of $CoCr_{2-x}Ce_xO_4$ ($x = 0$ to 0.02) that was synthesised utilising a solution combustion technique was investigated here. In order to determine whether or not the electrical response of rare earth doped samples altered as a function of relative humidity, research was conducted on the samples with the end goal of employing the samples as humidity sensors.

2 $CoCr_{2-x}Ce_xO_4$ ($x = 0$ to 0.02) synthesis procedure

2.1 Materials and synthesis

$CoCr_{2-x}Ce_xO_4$ ($x = 0$ to 0.020) were prepared y solution combustion method by using metal nitrates such as $Co[NO_3]6H_2O$, $Cr[NO_3]_39H_2O$, $Ce[NO_3]_39H_2O$ and fuels $C_6H_{12}O_6$ and NH_2CONH_2. The reducing agents (fuels) and oxidizers (metal nitrates) were kept at a 1:1 ratio in this synthesis. To generate a homogenous solution, the stoichiometry amount of needed metal nitrates and fuels were placed in a glass beaker and stirred constantly for around 45 min using a magnetic stirrer at 800 rpm. This homogeneous solution was

held at 450 °C within the muffle furnace. The fluid was initially boiled, frothed, and then burned.

2.2 Characterisation

The samples were characterized by powder X-ray diffraction using "PANalytical X'Pert Pro MPD" diffractometer (Cu-K$_\alpha$ radiation, Ni filter). The diffraction data were recorded in the detector angle (2θ) range of 10–80° with a step size of 0.02°.

The microstructure of the samples were investigated by scanning electron microscopy (SEM). The JEOL instrument was used in the collection of the SEM spectra (model JSM-840).

From the FTIR spectroscopy we can find the information about the position of ions in the crystal and about the inter atomic vibration modes of the samples using Agilent FTIR spectra.

For humidity sensing analysis, the powdered samples are pressed into pellets with a diameter of 10 mm through a hydraulic press (Fig. 1). To ensure ohmic contact, the obtained pellet sample was covered in silver paste. The sample covered by the silver electrode was positioned in the middle of the probes. The digital multimeter was linked to the probe's unconnected end at one end. In each flask that contained saturated salt solutions, the holder that contained the sample pellet was maintained there.

3 Results and discussions

3.1 Analysis of structure

XRD pattern of CoCr$_{2-x}$Ce$_x$O$_4$ ($x = 0$ to 0.02) as shown in the Fig. 2. The data are collected by exposing a sample to Cu-K radiation ($\lambda = 1.5418$). (Rigaku Corporation, Tokyo, Japan). The XRD patterns of CoCrCe reveal diffraction peaks are indexed to a cubic spinel structure of AB$_2$O$_4$. The peaks (220), (311), (222), (400), (422), (511), and (440) are indicating the cubic phase. The observed XRD patterns of CoCr$_2$O$_4$ were compared with the Joint Committee on Powder Diffraction Standards data that matches well with file(JCPDS Card No. 780711). The intensity of the diffraction peaks can be used to make inferences about changes in morphology and particle size, assuming this is done correctly. The Debye–Scherrer formula, which can be seen in Eq. 1 [27], was utilised in order to ascertain the dimensions of the crystals.

$$D = \frac{K\lambda}{\beta \cos\theta},$$ (1)

where D is the size of the crystallite, β is the line broadening at full width half maximum (FWHM), θ is the Bragg angle, λ is the X-ray wavelength, and K is a dimensionless form factor with a value near to unity. The size of the crystal is decreases with increasing Ce^{3+} concentration .

Fig. 1 Molecular structure of oxidizers and fuel use of synthesised element
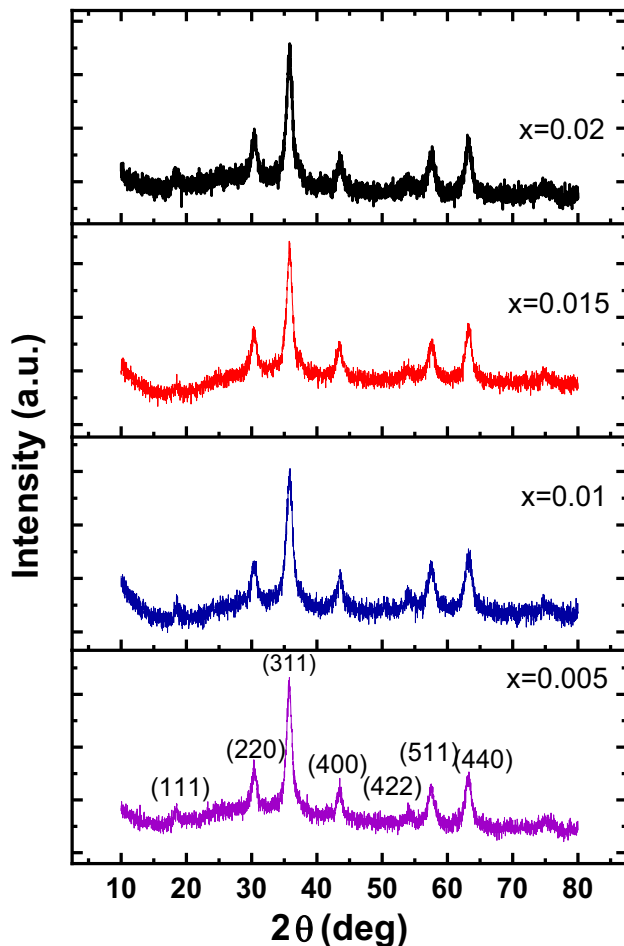

(Ce^{3+}-doped CoCr$_2$O$_4$ powder)
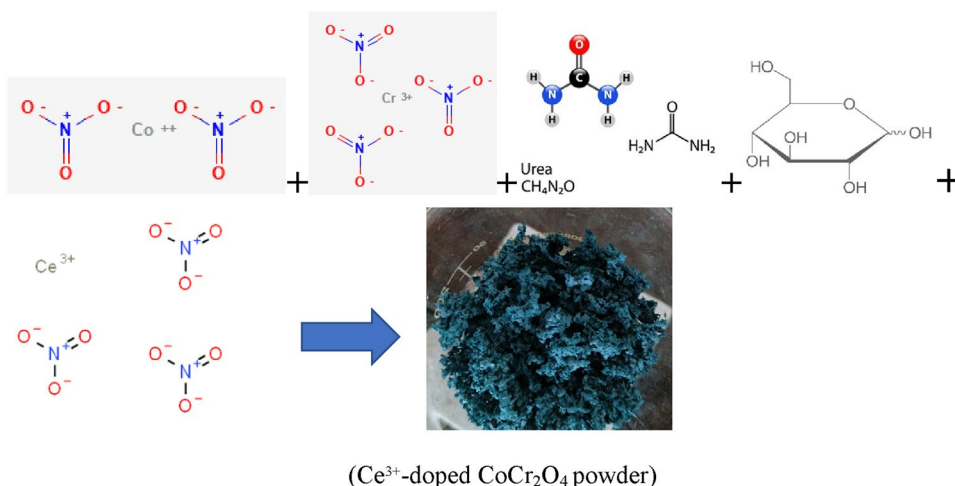
Fig. 2 XRD data of $CoCr_{2-x}Ce_xO_4$ [$x = 0$ to 0.02]

Latice parameter were calculated through the following formula [28].

$$d = a_0 \sqrt{h^2 + k^2 + l^2}$$
$$n\lambda = 2d \sin\theta \tag{2}$$

where, a_0 represents the lattice constant, d represents the distance between the atomic layers of the crystal, and (*hkl*) represents the plane indexing.

The values of lattice parameter were found in the range from 8.3289 and 8.3163 Å, respectively, were found to be the estimated lattice parameters for CoCrCe, which agree with the findings of earlier investigations.

Further Strain ε (%) of the samples are calculated by using Eq. 3

$$\text{Strain } \varepsilon(\%) = \frac{\beta}{4\tan\theta}, \tag{3}$$

Strain of sample increases after doping may be due to decrease in particle size. Further hoping lengths of the samples were calculated by using Eqs. 4 and 5. Hopping lengths in tetrahedral site L_A and octahedral site L_B are calculated based on the distance between magnetic ions.

$$L_A = 0.25 \, a\sqrt{3} \tag{4}$$

$$L_B = 0.25 \, a \sqrt{2}. \tag{5}$$

Table 1 provides the calculated values for L_A and L_B., lattice parameter, crystallite size and strain. As Ce^{3+} content "x" increases, the distance between magnetic ions decreasing. This can be explained by the disparity in ionic radii between the constituent ions.

3.2 Microstructural elementary analysis

Morphology of the samples is depicted in Fig. 3. The structure is composition dependant, according to SEM micrographs all samples shown higly porous nature, but no interior pores and a large number of intergrain holes. The Ce^{3+} ions-containing sample formed by self combustion had the finest granulation and a tendency to agglomerate particles. Furthermore, the intergranular pores are linked by the big pores. The pore structure is a network of interconnected spaces that create capillary tubes [29]. The amount of Co,

Table 1 Data obtained from XRD such as crystallite size, unit cell volume, lattice parameter

Ce^{3+} content x	lattice parameter (Å)	Crystallite Size D in (nm)	Volume (Å^3)	Strain ε (%)	Hoping length (Å) L_A	L_B
0	8.3289	15	578	1.4317	3.6065	2.9447
0.005	8.3260	13	577	1.3063	3.6052	2.9437
0.01	8.3194	12	575	1.3724	3.6024	2.9413
0.015	8.3180	11	576	1.3823	3.6018	2.9408
0.02	8.3163	10	575	1.541	3.6010	2.9402

Cr, Ce^{3+}, and O in the compositions were determined using energy dispersive X-ray spectroscopy. The graphs are depicted in Fig. 3. The components are present in roughly the same stoichiometric amount as when stored in pure water, according to the chemical makeup, with no substantial impurities.

3.3 Fourier infrared spectroscopy analysis

Figure 4 depicts FTIR spectra of nanocrystalline $CoCr_{2-x}Ce_xO_4$ [x = 0 to 0.02] obtained at room temperature in the frequency range 400–4000 cm^{-1}. FTIR confirm the spinel structure of of $CoCr_{2-x}Ce_xO_4$[x = 0 to 0.02], which consists of two sharp bands v_1 and v_2 in the wavenumber range 400–600 cm^{-1}. The cation distribution of tetrahedral and octahedral sites determines the characteristics of $CoCr_{2-x}Ce_xO_4$. The vibrational modes are represented by the lower wave number sidebands in the FTIR spectra. Two sharp frequency bands, v_1 (589 cm^{-1}) and v_2 (440 $^{-1}$), confirm the synthesis of spinel chromite, which occurs as a result of Cr^{3+}-O_2 stretching vibration at tetrahedral and octahedral sites [5, 24, 30, 31].

3.4 Variation of the relative permittivity against relative humidity

The humidity is the most crucial parameter, which shows its effect on the operation of electronic devices. Hence its very important to record the humidity level of the environment and to note its effects on measured parameters. In this paper for the first time, the variation of the electrical conductivity with the relative humidity was recorded for the (CoCrCe) samples. The conductivity behaviour of these samples was tested at ambient room temperature with in the relative humidity ranging from 0 to 98% RH levels respectively which gives definite relative humidity are used [32]. For the measurement we have used saturated salts solutions such as Lithium chloride (LiCl), Potassium acetate [K(CH$_3$COO)], Magnesium chloride (MgCl$_2$), Potassium carbonate (K$_2$CO$_3$), Magnesium nitrate [Mg(NO$_3$)$_2$], Sodium chloride (NaCl), Potassium chloride (KCl) and potassium sulfate (K$_2$SO$_4$) at 28 °C.

The Fig. 5 depicts the variation of the electrical permittivity with the relative humidity of the (CoCrCe) samples for different compositions (x = 0.0, 0.005, 0.010, 0.015 and 0.020). The plots clearly depict that, as the relative humidity increases the relative permittivity also increases and it is maximum for the $CoCr_{2-x}Ce_xO_4$

(x = 0.02) sample. Also, at higher humidity level more enhancement in the permittivity of the samples is observed. The possible mechanism to explain the resistive and capacitve and its relation to the humidity of the Cobalt chromate and how the substitution by foreign element influence the related mechanism is Cerium(Rare earth with larger ionic radii) contributes to the increase of the effective surface of the material exposed to water vapours by increasing the porosity of the material and the permittivity of the chromate material, thereby favouring the conduction processes on the effective surface of the material exposed to humidity.
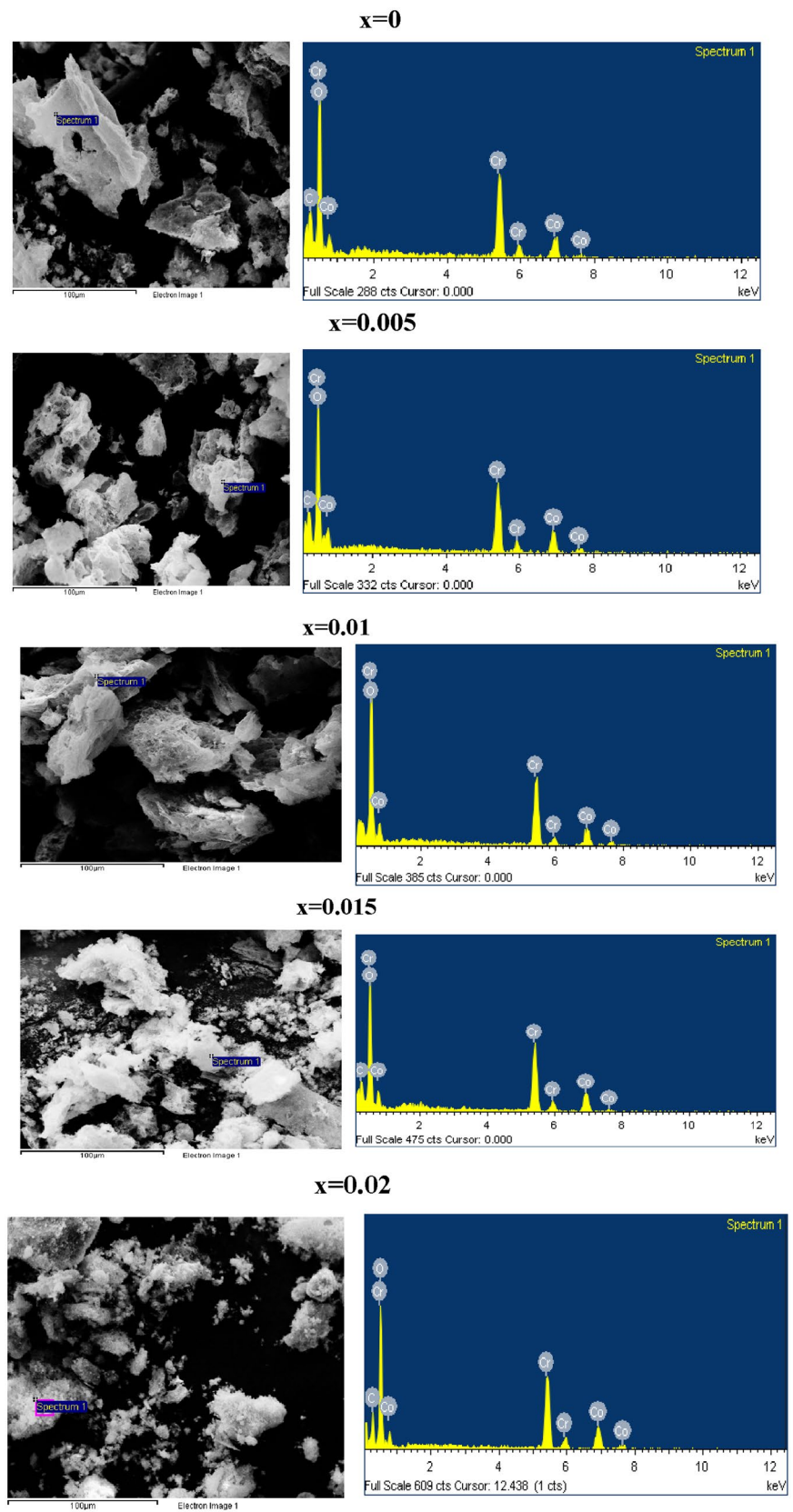
3.5 Conductivity against relative humidity

The change in the electrical conductivity with relative humidity was shown in Fig. 6. The electrical resistance of the $CoCr_{2-x}Ce_xO_4$ (x = 0.0, 0.005, 0.010, 0.015 and 0.020) samples shows that, as the relative humidity increases the conductivity decreases. At lower humidity the conductivity is high [33]. The possible mechanism to explain the conductivity is increases with Ce^{3+} contributes to the increase of the effective surface of the material exposed to water vapours by increasing the porosity of the material and electrical conductivity of the chromate material, thereby favouring the conduction processes on the effective surface of the material exposed to humidity.

3.6 Electrical capacity and electrical resistance in normalised

The variation of the normalised electrical capacitance and normalised electrical resistance with the relative humidity at room temperature from 0 to 98% relative humidity were recorded and plotted in Figs. 7 and 8 respectively. Electrical conductivity is found highest for Ce^{3+} = 0.02 concentration due to larger ionic radius of the Ce^{3+} compare to Cr.

The Fig. 7 clearly depicts that below 40% relative humidity the co-efficient of C/C_0 indicates less sensitivity but as the relative humidity more that 40%, the samples show good sensitivity. This good sensitivity for $CoCr_{2-x}Ce_xO_4$ (x = 0.015) sample may be due to the more porous structure of the sample and decreased crystallite size. The Fig. 8 show that, as the relative humidity increases the co-efficient of resistance R/R_o decrease, which intern represents that at lower

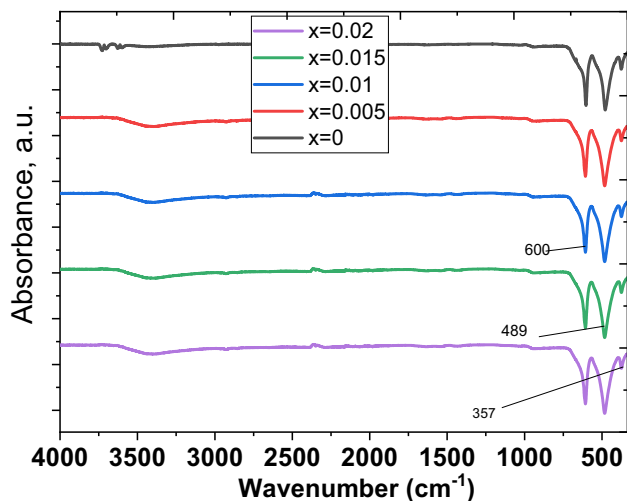**Fig. 3** SEM micrographs and EDS pattern of $CoCr_{2-x}Ce_xO_4[x = 0$ to $0.02]$

Fig. 4 FTIR spectra of the CoCr$_{2-x}$Ce$_x$O$_4$[$x=0$ to 0.02]

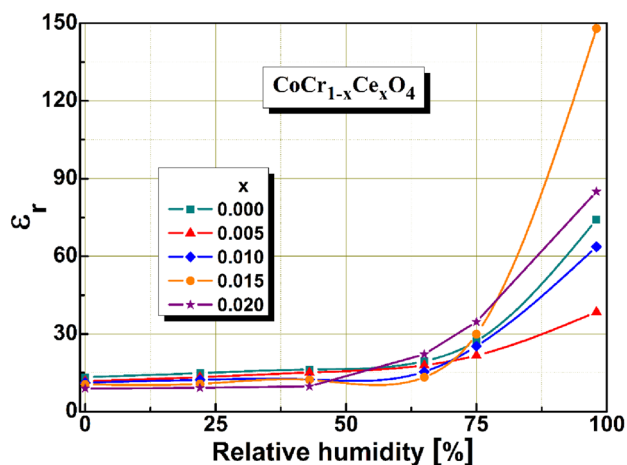Fig. 6 The variation of the conductivity against relative humidity at the constant frequency of 1 kHz

Fig. 5 The variation of the relative permittivity against relative humidity at the constant frequency of 1 kHz

Fig. 7 The variation of the electrical capacity in normalised form for the CoCr$_{2-x}$Ce$_x$O$_4$ ($x=0.005$, 0.010, 0.015 and 0.020) samples at the constant frequency of 1 kHz

humidity the sensitivity of the sample's is good but at higher humidity the sensitivity is poor.

3.7 Response time of capacitive sensor and resistive sensor

The timing behaviour is one of the important parameters to judge the potentiality of the sensor. In the present study response time was examined for the CoCr$_{2-x}$Ce$_x$O$_4$ samples over a humidity range of 0–98% at room temperature. The response time was measure for the variation in resistive (electrical conductivity) and capacitance (electrical permittivity). The Fig. 9
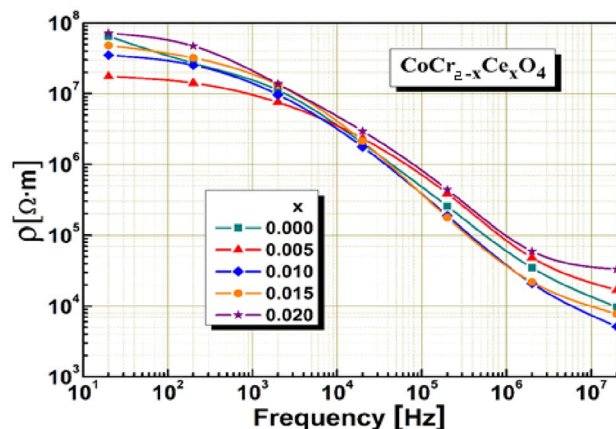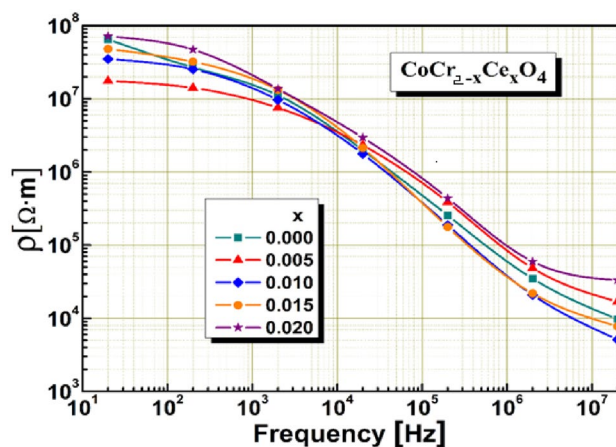
depicts that drastic variation on the response time for electrical permittivity was observed by changing the relative humidity from lower to higher humidity. More variation the permittivity was observed for all the samples, but the CoCr$_{2-x}$Ce$_x$O$_4$ ($x = 0.015$) sample showed a drastic variation of the response time, this may be due to the synergistic effects and porous nature of the sample.

The Fig. 10 clearly gives the response timing behaviour of the electrical conductivity of the samples. The response time for electrical conductivity varies more significantly. The magnitude of two order change in the electrical conductivity was observed for CoCr$_{2-x}$Ce$_x$O$_4$ samples. Among these samples the

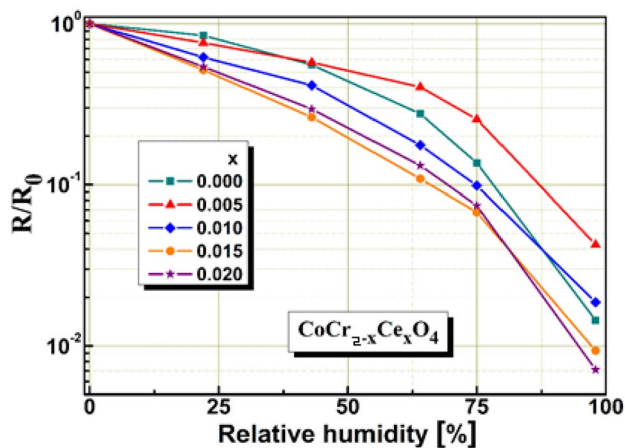**Fig. 8** The variation of the electrical resistance in normalised form for the $CoCr_{2-x}Ce_xO_4$ ($x = 0.005$, 0.010, 0.015 and 0.020) samples at the constant frequency of 1 kHz

Fig. 10 The response time of resistive sensor for $CoCr_{2-x}Ce_xO_4$ samples

$CoCr_{2-x}Ce_xO_4$ ($x = 0.015$) has shown a drastic variation. This may be due to the enlarged surface area and maximum porous nature of the sample.

This study gives a new way to the research about the electrical conductivity study with the variation in the humidity. There are fever literatures are available related to this work. The $CoCr_{2-x}Ce_xO_4$ samples has shown better variation in the conductivity as the humidity changes from 0 to 98% at ambient temperature. Among the prepared samples $CoCr_{2-x}Ce_xO_4$ ($x = 0.015$) sample has shown good sensitivity and better response to the change in the humidity.
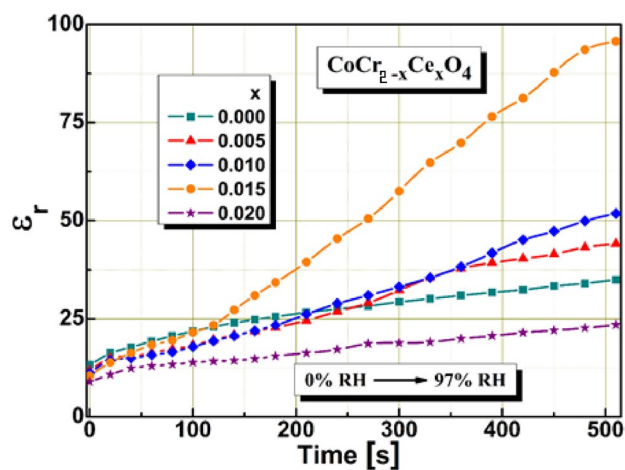
4 Conclusion

In this work, Ce^{3+} doped and undoped $CoCr_2O_4$ powder was successfully generated by solution combustion method using glucose and urea as fuels for the first time ever. This is the first study of its type. In this work, we looked examined how the presence of Ce^{3+} affected the structural, spectroscopic, and humidity sensing capabilities of $CoCr_2O_4$. The resistivity drops even further as the crystallite size gets smaller, with the maximum resistivity being reached in samples that have the highest granulation but a lower dopant concentration. The Ce^{3+} substitution contributes to a drop in electrical resistivity, which puts the material's resistivity into the measurable zone. This is advantageous for applications using sensors because of the material's increased ability to be measured. The possible mechanism to explain the resistive and capacitve and its relation to the humidity of the Cobalt chromate and how the substitution by foreign element influence the related mechanism is Cerium(Rare earth with larger ionic radii) contributes to the increase of the effective surface of the material exposed to water vapours by increasing the porosity of the material and the permittivity and electrical conductivity of the chromate material, thereby favouring the conduction processes on the effective surface of the material exposed to humidity. The ratio of Ce^{3+} can be chosen to optimize the response of the corresponding electrical parameter (permittivity or conductivity) under the influence of humidity based on the type of sensor considered (capacitive or resistive).

Fig. 9 Relative permittivity v/s response time of capacitive sensor for $CoCr_{2-x}Ce_xO_4$ samples

Author contributions

JAV: Conceptualization, Methodology, Software and Writing—Original Draft preparation and editing, KA: Analysis, NL: Analysis, AHH: Editing, NB: Editing, Conceptualization.

Declarations

Competing interest The authors declare that they have no known competing financial interests or personal relationships that could have appeared to influence the work reported in this paper.

References

1. N. Yamazoe, Y. Shimizu, Humidity sensors: principles and applications. Sens. Actuators **10**, 379–398 (1986)
2. H. Farahani, R. Wagiran, M.N. Hamidon, Humidity sensors principle, mechanism, and fabrication technologies: a comprehensive review. Sensors. **14**, 7881–7939 (2014)
3. M. Pelino, C. Cantalini, M. Faccio, Principles and applications of ceramic humidity sensors. Act. Passiv Electron. Compon. **16**, 69–87 (1994)
4. K. Manjunatha, V. Jagadeesha Angadi, M.C. Oliveira, S.R. de Lazaro, E. Longo, R.A.P. Ribeiro, S.O. Manjunatha, N.H. Ayachit, Towards shape-oriented bi-doped $CoCr_2O_4$ nanoparticles from theoretical and experimental perspective: structural, morphological, optical, electrical and magnetic properties. J. Mater. Chem. C **9**, 6452–6469 (2021)
5. I. Petrila, F. Tudorache, S. Tascu, Micromagnetic investigation of all-optical switching. Phys. Lett. A **377**, 1495–1498 (2013)
6. K. Manjunatha, V. Jagadeesha Angadi, R. Rajaramakrishna, U. Mahaboob, Pasha, Role of 5 mol% Mg–Ni on the structural and magnetic properties of cobalt chromates crystallites prepared by solution combustion technique. J. Supercond. Nov. Magn. **33**, 2861–2866 (2020)
7. K. Manjunatha, V. Jagadeesha Angadi, K.M. Srinivasamurthy, S. Matteppanavar, V.K. Pattar, Mahaboob Pasha, exploring the structural, dielectric and magnetic properties of 5 Mol% Bi^{3+}-Substituted $CoCr_2O_4$ nanoparticles. J. Supercond Nov Magn. **33**, 1747–1757 (2020)
8. I. Petrila, V. Manta, Metropolis Monte Carlo analysis of all-optical switching. Comput. Phys. Commun. **185**, 2874–2878 (2014)
9. I. Petrila, F. Ungureanu, V. Manta, Effects of laser beam modulation on all-optical switching phase diagrams in magneto-optical ultrafast storage device. J. Comput. Electron. **14**, 627–633 (2015)
10. K.K. Bharathi, J.A. Chelvane, G. Markandeyulu, Magnetoelectric properties of Gd and Nd-doped nickel ferrite. J. Magn. Magn. Mater. **321**, 3677–3680 (2009)
11. S. Chikazumi, *Physics of ferromagnetism* (Oxford University Press Inc, New York, 1997)
12. F. Tudorache, I. Petrila, Effects of partial replacement of Iron with Tungsten on microstructure, electrical, magnetic and humidity properties of copper-zinc ferrite material. J. Electron. Mater. **43**, 3522–3526 (2014)
13. K. Wu, Y. Lu, Y. Liu, Y. Liu, M. Shen, M. Debliquy, C. Zhang, Synthesis and acetone sensing properties of copper (Cu^{2+}) substituted zinc ferrite hollow micro-nanospheres. Ceram. Int. **46**(18), 28835–28843 (2020)
14. I. Petrila, F. Tudorache, Influence of partial substitution of Fe^{3+} with W^{3+} on the microstructure, humidity sensitivity, magnetic and electrical properties of barium hexaferrite. Superlattices Microstruct. **70**, 46–53 (2014)
15. K. Manjunatha, V. Jagadeesha Angadi, R.A.P. Ribeiro, M.C. Oliveira, S.R. de Lázaro, M.R.D. Bomio, S. Matteppanavar, S. Rayaprol, P.D. Babu, Structural, electronic and magnetic properties of Sc^{3+} doped $CoCr_2O_4$ nanoparticles. New J. Chem. **44**, 14246–14255 (2020)
16. P. Thamilmaran, M. Arunachalam, S. Sankarrajan, K. Sakthipandi, M. Sivabharathy, Structural transition in Gd doped $LaCrO_3$ isovalent by in-situ ultrasonic measurements. Phys. B Condens. Matter **530**, 270–276 (2018)
17. R.R. Kanna, K. Sakthipandi, N. Lenin et al., Neodymium doped on the manganese–copper nanoferrites: analysis of structural, optical, dielectric and magnetic properties. J. Mater. Sci. Mater. Electron. **30**, 4473–4486 (2019)

18. N. Betancur-Granados, O.J. Restrepo-Baena, Flame spray pyrolysis synthesis of ceramic nanopigments $CoCr_2O_4$: the effect of key variables. J. Eur. Ceram. Soc. **37**, 5051–5056 (2017)

19. K. Manjunatha, V.J. Angadi, A.P. Renan, E. Ribeiro, M.C. Longo, R.D. Oliveira, Mauricio, R. Bomio, Sergio, S. de Lazaro, S. Matteppanavar, P.D. Rayaprol, M. Pasha, Structural, electronic, vibrational and magnetic properties of Zn^{2+} substituted $MnCr_2O_4$ nanoparticles. J. Magn. Magn. Mater. **502**, 166595 (2020)

20. V. Jagadeesha Angadi, K. Manjunatha, K. Praveena, V.K. Pattar, B.J. Fernandes, S.O. Manjunatha, J. Husain, S.V. Angadi, L.D. Horakeri, K.P. Ramesh, Magnetic properties of larger ionic radii samarium and gadalonium doped manganese zinc ferrite nanoparticles prepared by solution combustion method. J. Magn. Magn. Mater. **529**, 167899 (2021)

21. P. Pankaj Choudhary, A. Saxena, V.N. Yadav, A. Rai, Mishra, Dielectric and ferroelectric properties of $CoCr_2O_4$ nanoceramics. J. Adv. Dielectr. **9**, 1950015 (2019)

22. K. Manjunatha, V.J. Angadi, B.J. Fernandes, K.P. Ramesh, *Synthesis and study of structural and dielectric properties of Dy-Ho doped Mn-Zn ferrite nanoparticles* (Intech Open publishers, London, 2021)

23. V. Jagadeesha Angadi, K. Manjunatha, M. Akyol, A. Ekicibil, S. Matteppanavar, A.V. Pavlenko, S.P. Kubrin, Temperature-dependent dielectric and magnetic properties of scandium-substituted $HoFeO_3$ nanoparticles. J. Supercond. Nov. Magn. **33**, 3525–3534 (2020)

24. S. Pavithradevi, N. Suriyanarayanan, T. Boobalan, Synthesis, structural, dielectric and magnetic properties of polyol assisted copper ferrite nano particles. J. Magn. Magn. Mater. **426**, 137–143 (2017)

25. K. Ali, J. Iqbal, T. Jan, I. Ahmad, D. Wan, I. Ahmad, Influence of NiO concentration on structural, dielectric and magnetic properties of core/shell $CuFe_2O_4$/NiO nanocomposites. Mater. Chem. Phys. **195**, 283–294 (2017)

26. K. Manjunatha, K.M. Srininivasamurthy, C.S. Naveen, Y.T. Ravikiran, E.I. Sitalo, S.P. Kubrin, S. Matteppanavar, N. Sivasankara Reddy, J. Angadi, Observation of enhanced humidity sensing performance and structure, dielectric, optical and DC conductivity studies of scandium doped cobalt chromate. J. Mater. Sci. Mater. Electron. **30**, 17202–17217 (2019)

27. P. Samoila, T. Slatineanu, P. Postolache, A.R. Iordan, M.N. Palamaru, The effect of chelating/combustion agent on catalytic activity and magnetic properties of Dy doped Ni–Zn ferrite. Mater. Chem. Phys. **136**, 241–246 (2012)

28. R. Sharma, S. Singhal, Structural, magnetic and electrical properties of zinc doped nickel ferrite and their application in photo catalytic degradation of methylene blue. Phys. B **414**, 83–90 (2013)

29. F. Tudorache, I. Petrila, K. Popa, A.M. Catargiu, Electrical properties and humidity sensor characteristics of lead hydroxyapatite material. Appl. Surf. Sci. **303**, 175–179 (2014)

30. F. Tudorache, I. Petrila, P.D. Popa, S. Tascu, Influence of thermal treatment on the structure, humidity sensitivity, electrical and magnetic properties of barium–tungsten ferrite. Compos. B Eng. **51**, 106–111 (2013)

31. I. Petrilaa, F. Tudorache, Effects of sintering temperature on the microstructure, electrical and magnetic characteristics of copper-zinc spinel ferrite with possibility use as humidity sensors. Sens. Actuators: Phys. **332**, 113060 (2021)

32. F. Tudorache, Investigations on microstructure, electrical and magnetic properties of copper spinel ferrite with WO_3 addition for applications in the humidity sensors, superlattices and microstructures. Res Data Policy Data Availab Statements **116**, 131e140 (2018)

33. M.-K. Ho, H.-H. Chiu, T.-E. Hsu, B. Chethan, S.-L. Yu, C.-Y. Jheng, C.-E. Chin, R. Selvam, C.-L. Cheng, H. Nagabhushana, K. Manjunatha, Advancing humidity sensing and magnetocaloric properties of spinel structural $CoCr_2O_4$ nanoparticles achieved via innovative bismuth doping by combustion synthesis. Mater. Today Chem. **35**, 101907 (2024). https://doi.org/10.1016/j.mtchem.2024.101907